Author/s:
Dong, Y;Akinoglu, EM;Zhang, H;Maasoumi, F;Zhou, J;Mulvaney, P

Title:
An Optically Responsive Soft Etalon Based on Ultrathin Cellulose Hydrogels

Date:
2019-10-01

Citation:
Dong, Y., Akinoglu, E. M., Zhang, H., Maasoumi, F., Zhou, J. & Mulvaney, P. (2019). An Optically Responsive Soft Etalon Based on Ultrathin Cellulose Hydrogels. Advanced Functional Materials, 29 (40), https://doi.org/10.1002/adfm.201904290.

An Optically Responsive Soft Etalon Based on Ultrathin Cellulose Hydrogels

Yue Dong, Eser Metin Akinoglu, Heyou Zhang, Fatemeh Maasoumi, Jinping Zhou and Paul Mulvaney**

Dr. Y. Dong, Dr. E. M. Akinoglu, H.-Y. Zhang, Dr. F. Maasoumi, Prof. Paul Mulvaney

ARC Centre of Excellence in Exciton Science, School of Chemistry, University of Melbourne, Parkville, Victoria 3010, Australia

E-mail: mulvaney@unimelb.edu.au

Dr. Y. Dong, Prof. J.-P. Zhou

Department of Chemistry and Key Laboratory for Biomedical Polymers, Ministry of Education, Wuhan University, Wuhan 430072, China

E-mail: zhoujp325@whu.edu.cn

Abstract:

Stimuli responsive optical etalons are an exciting class of next-generation sensors because they are scalable, cost-effective and offer tunability of their optical response across the entire UV-Vis-NIR wavelength range. In this study, double-network cellulose hydrogels are used as a soft, responsive medium and are incorporated into Fabry-Pérot optical etalons. The thin

cellulose hydrogel layer can be solution processed. The hygroscopic hydrogel undergoes both refractive index and thickness changes in response to changes in humidity. This leads to strong changes in reflection due to optical interference within the MIM cavity. The response can be optimized by adjusting the chemical crosslinker ratio. These flexible MIM structures provide a robust platform for optically based chemical sensors.

Keywords: MIM devices, soft etalon, cellulose, hydrogels, Fabry-Pérot, humidity sensor.

1. Introduction

Mechanically responsive polymers provide a broad platform for the development of smart materials and have been integrated into a variety of optical filters, sensors, indicators and diodes.[1] Of particular interest is the transduction of the mechanical response into an optical signal. For example, polymer based photonic crystals exhibit strong colour changes when the periodicity of the structure is altered by an external stimulus. However it is difficult to routinely fabricate such high quality photonic crystals. Here we consider the simpler and more scalable case of metal-insulator-metal (MIM) thin films. These are well established optical structures and are used in lasing applications,[2,3] as light absorbers,[4-6] and as etalons[7,8]. MIM structures usually comprise thin-film stacks of rigid materials with semiconductor alloys[2], metallic oxides[9,10] or metal nitrides[11] as the insulating layer. More recently, soft materials including liquids[12], polysiloxane[13], PDMS[14], silk protein[15] and polyimide[16], have also been used as

the insulating layer, in order to introduce flexibility. Nevertheless, it is still challenging to create stimuli-responsive materials within optical MIM structures.[17] Here, we use cellulose hydrogels as the swellable active layer, which enables active colour-shifting.[18] The advantage of such bio-hydrogels is that they are soft (Young's moduli < 10^5 N/m^2), water-permeable, eco-friendly, and compatible with many other materials and applications.[19-21] Hydrogels have been used in drug delivery platforms,[22,23] as tissue scaffolds,[24,25] in water purification systems,[26,27] electric power generation[28, 29] and colour actuation sensing[30,31]. A key advantage is that careful chemical modification of the hydrogel precursors enables control of the mechanical strength and elasticity of the resultant films. Recently, double-network (DN) based hydrogels made from polysaccharides have begun to replace both traditional, covalent DN hydrogels and reinforced, single-network hydrogels, due to their high strength, toughness and transparency.[32] [33] In most cases, the resultant materials are colourless because cellulose itself does not absorb visible light, nor does it scatter light significantly.[34] However, structural colour can be generated by introducing periodic, subwavelength structures. [35,36] To exemplify this, we report here on flexible Fabry-Pérot type etalons for humidity sensing. [37] [38] To quantify the optical response of the sensor, we have also carried out COMSOL simulations and we show that these reproduce the experimental results accurately.

2. Results and discussion

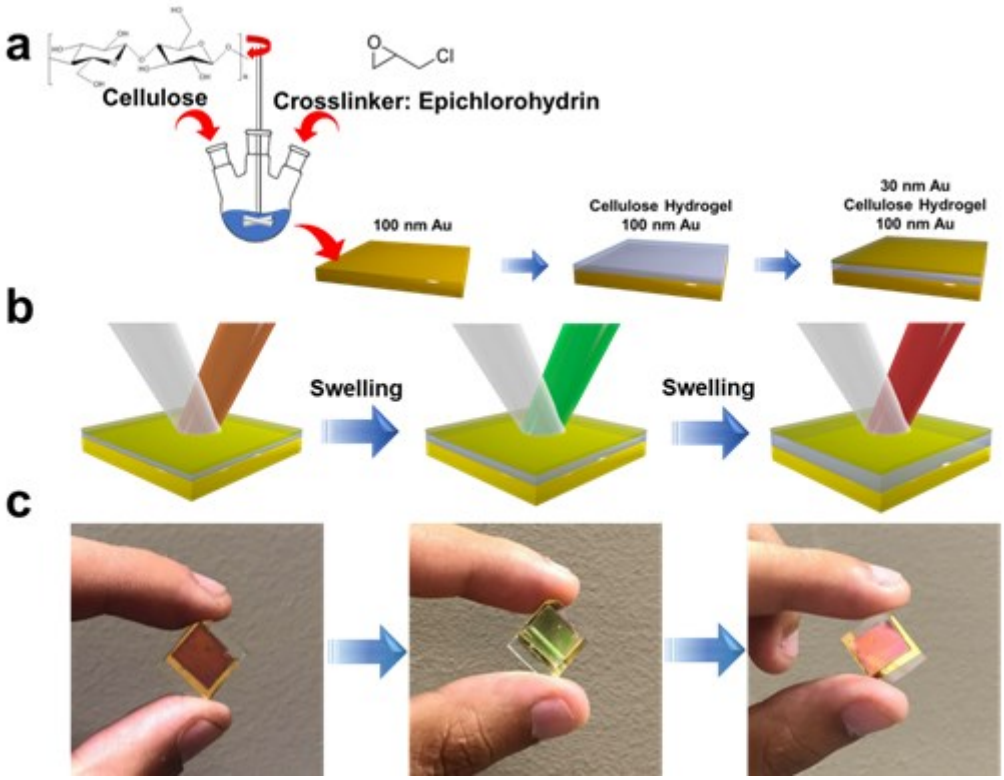

Figure 1. (a) Schematic fabrication process of the planar hydrogel MIM etalon. (b) Scheme illustrating the colour changes observed in reflected light following swelling of the film, due to increases in cellulose hydration. (c) Photographs of the planar hydrogel MIM etalon before, during and after immersion into distilled water for 1 h at 20 ± 3 °C with ambient humidity of 30 ± 5 %. Here, the ECH:AGU ratio is 3. The thickness of the dried hydrogel film is 170 ± 7 nm.

The fabrication of the planar Au/cellulose/Au film stacks is illustrated in Figure 1. An optically thick 100 nm Au film serves as a base layer on which the cellulose hydrogel precursors are spin coated. The concentration of the cellulose solution is adjusted to ensure that the viscosity is suitable for spin coating at high spin speeds. Formation of long-range continuous networks in the hydrogel film is guaranteed by the large (weight-average) molecular-weight of cellulose: 100 kDa. Chemical cross-linking occurs due to etherification between cellulose and epichlorohydrin, ECH (Scheme S1). This double-network cellulose based hydrogel is a simple,

abundant and inexpensive material with superior mechanical properties including high strength and toughness, which endows the film with good mechanical stability.[42] Upon drying, the cellulose hydrogel forms a film and it is then coated with 30 nm Au to finalize the MIM thin film stack architecture. Figures 1b and 1c present the scheme and photographs of the planar MIM film stacks before, during and after swelling with water. The optical response is strongly dependent on the insulator film thickness. A distinct change in colour can be observed as the cellulose film transitions from the compressed, dry state (red-orange) to the fully swollen and wet state (bright red) via a continuum of semi-swollen states (green tones).

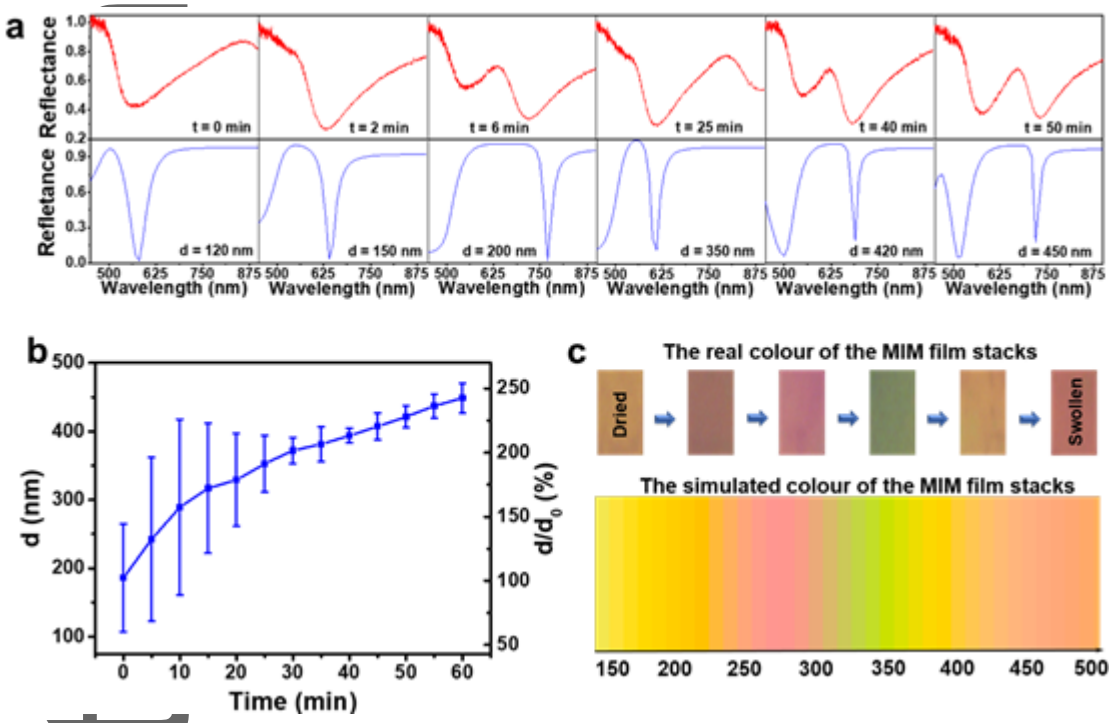

Figure 2. (a) Evolution of the measured (top line) and simulated (bottom line) reflection spectra of an MIM etalon as it progresses from the dry state to the fully swollen state. (*t* represents the time of swelling; *d* represents the thickness of the insulator layer in the simulations) (b) A plot of the average thickness *d* (nm) of the hydrogel film as a function of the immersion time in distilled water. The molar ratio of epichlorohydrin (ECH) to

anhydroglucose units (AGU) in the cellulose gel is 3. The error bars represent the standard deviation from 5 samples. (c) The visible colour of the planar MIM film stacks converted to RGB/XYZ Matrix values from experimental spectra (top) and from the simulated spectra (bottom). The CIE standard illuminate D65 was used as the white reference. The thickness of the dry hydrogel film was 170 ± 7 nm.

The effects of the cellulose hydrogel swelling on the optical response are shown in Figure 2. Measured reflection spectra collected from a representative sample are shown in Figure 2a (top line) to illustrate how the optical signature evolves during swelling over 50 min. It can be seen that there is initially a single reflection minimum, which gradually red-shifts as the film swells. Later, a second and then third minimum also appear in the spectra. This is the typical optical response of a Fabry-Pérot cavity in reflection. In general, the minima are associated with destructive interference and they occur when the phase shift satisfies

$$\delta = (2m\text{-}1)\pi \qquad m = 1,2,3\ldots \tag{1}$$

Here m indicates the order of the interference and

$$\delta = \frac{2\pi nd}{\lambda}\cos(\theta) \tag{2}$$

is the phase shift. Here n is the refractive index of the cellulose hydrogel, d is the insulator film thickness, θ is the angle of incidence, and λ is the in vacuum wavelength of the incident light. From Equation 2 it follows that, for constant n and d, there must be certain wavelengths λ that will destructively interfere and will be filtered out of the spectrum. This is the origin of the minima in the reflection spectra. Furthermore, an increase in d implies an increase in λ to meet the interference condition in Equation (1). Hence, the minima must shift to the red as the film thickness increases. The appearance of the second and third minima results from higher order resonances moving into the visible spectral range. These minima were previously located in the UV region. In the lower line of Figure 2(a) we present the corresponding simulated spectra,

which show excellent agreement with the experiments. These were obtained by feeding the wavelength-dependent refractive index of the materials and the measured film thicknesses into the Fresnel equations. For the complex refractive index of gold metal, we have used data from literature.[24] In the case of the cellulose hydrogel it is important to account for the fact that the refractive index will change with water content. For the dry cellulose film, the refractive index was obtained from ellipsometry measurements (Figure S2a). To approximate the refractive index of the cellulose hydrogel with different water volume-fractions, we treat it as a homogeneous effective medium. The refractive index of the hydrated cellulose hydrogel n_{eff} (Figure S2b) can be estimated from the measured refractive index of the dry cellulose film n_c = 1.53 and the refractive index of water n_w = 1.33 using the Maxwell-Garnett approximation. This results in the following effective refractive index:

$$n_{eff}(h) = \sqrt{\varepsilon_c \frac{\varepsilon_c + \frac{1+1.08h}{3}(\varepsilon_w - \varepsilon_c)}{\varepsilon_c + \frac{1-0.54h}{3}(\varepsilon_w - \varepsilon_c)}}$$

where $\varepsilon = n^2$ is the respective relative optical permittivity. The hydration h provides a measure of the swelling and was derived from the relative thickness changes between the completely dry and completely swollen films. We measured five samples with a fixed ECH:AGU molar ratio of 3 and deposited at spin speeds of 8000 rpm for 5 min. The mean thickness of the dried hydrogel films was 186 ± 78 nm (Figure 2(b), t = 0). Furthermore, we found there was an average deviation in thickness of 30 nm across different areas of individual samples, which were 50 mm x 50 mm in size (Figure S3). When the MIM film stacks are immersed into water, they begin to swell. The evolution of the film thickness from the dry to the swollen state is shown in Figure 2b. It can be seen that there is a non-linear increase in the thickness over time. This is a consequence of the change in the driving force for water uptake into the hydrogel, which is at a maximum when the dry film contacts water. The swelling rate then decreases from its maximum rate of ~11nm/min to ~3 nm/min at the end of the uptake process (Figure S4). The

effects on the film colour are shown in Figure 2c. Here, the measured and simulated spectra from Figure 2b have been converted to CIE colour space with illuminant D65. The experimental spectra are thus transformed into the colours shown in the upper row and it is evident that the colour changes from orange to pink, then to green and finally to red. The simulated spectra and corresponding colour changes are shown in the lower row. (The colour changing route is also visualized in a chromaticity diagram in Figure S5.)

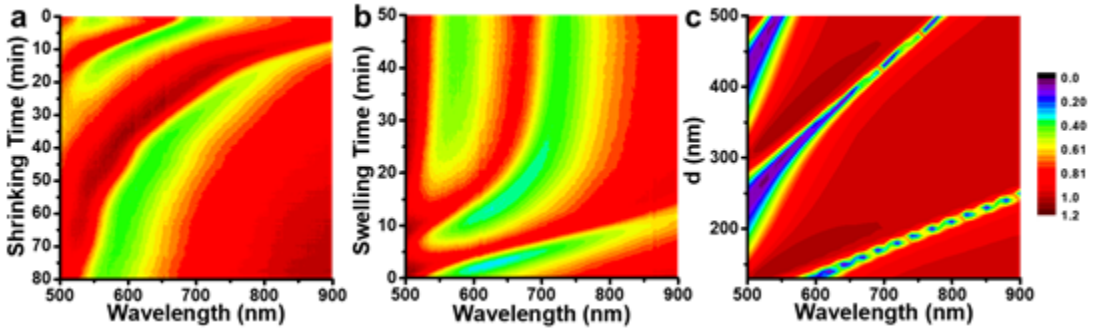

Figure 3. (a) Reflectance as a function of wavelength and time for a swollen, planar hydrogel MIM etalon after exposure to environmental humidity 30 ± 5% at room temperature. The reflectance spectrum at time = 0 min is the spectrum of the fully swollen device. The thickness decreases over time as the cellulose hydrogel loses water. (b) Reflectance as a function of wavelength and time for a planar hydrogel MIM etalon during the 11th swelling cycle. The molar ratio of ECH: AGU of cellulose is 3. The thickness of the dry hydrogel film is 170 ± 7 nm. (c) Simulated reflectance spectra for a planar hydrogel MIM etalon as a function of the layer thickness, calculated using COMSOL. The thickness of the insulator layer, d, ranges from 175 to 500 nm, while n, the refractive index of the insulator layer, ranges from 1.44 to 1.53. Reflectance is defined as the fraction of light emitted vertically for an incident beam normal to the surface. In the simulations, it is measured relative to the calculated reflectance of a thick gold film.

Reversibility of the optical signature changes and therefore the polymer network swelling behaviour is critical for practical applications. Figure 3 shows the reflection spectra of a MIM etalon with a 170 nm dried insulator layer as a function of shrinking or swelling time and wavelength. Here, the reflection intensity is colour coded and the positions of the minima are

indicated in green. The shrinking process (Figure 3a) starts at t = 0 min with two minima corresponding to $m = 1$ and $m = 2$ in Equation (1). As the shrinking progresses, the reflection minima blue-shift because of the decrease in insulator thickness. Within 10 min the higher order minimum moves out of the spectrum towards the UV region. Shortly after, a lower order minimum moves into the spectrum from the IR region. Eventually, this peak is the only minimum that remains in the spectrum. We note that the shrinking process is accompanied by a non-linear change in the thickness over time. This is evident from the nonlinear and sloping green strokes, which indicate the position of the minima. The shrinking is most rapid at the start of the process giving a fast reflectance minimum shift. Once dried, the reflectance dip remains at approximately 580 nm for this sample in agreement with the dried cellulose film data in Figure 2a. Subsequently, we exposed the film stack to 10 swelling and shrinking cycles. The spectral evolution during the 11th swelling process is shown in Figure 3b. It starts as a dry film at t = 0 min and shows the same optical signature as the dry states in previous cycles (Figure 3a & Figure 2a). The spectral evolution during the swelling process is reproduced, i.e. three minima of subsequent orders m, m+1 and m+2 move through the spectrum as the film thickness increases. Finally, the reflection spectra match the spectra obtained under the starting conditions (t = 0 min in Figure 3a), representing the fully swollen state. We use simulated reflection spectra with a linearly increasing evolution of the insulator thickness to illustrate the process more clearly in Figure 3c. Note that in the simulations, the minima appear purple and blue because the simulations yield idealized spectra with sharper resonances. A comparison of the measured and simulated spectra reveals that Figure 3a and Figure 3b are equivalent to Figure 3c with distortions along the y-axis. Video S1 visualizes the color change during the shrinking and swelling processes. The videos show a high-contrast colour change associated with hydrogel thickness change.

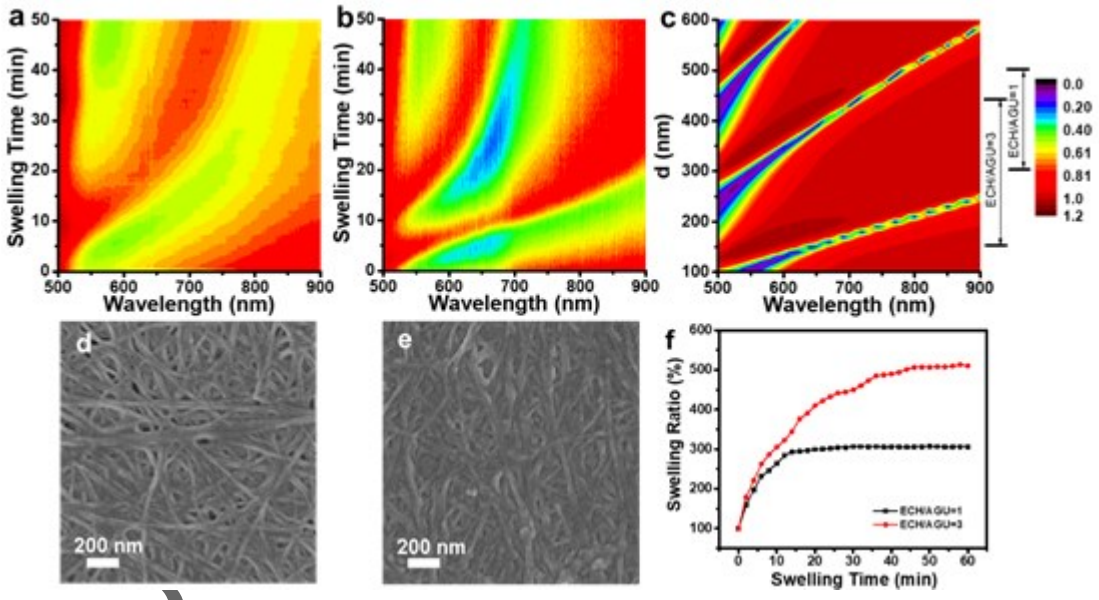

Figure 4. Reflectance as a function of wavelength and swelling time for planar hydrogel MIM etalons with two different ECH:AGU ratios: (a) ECH:AGU = 1 and (b) ECH:AGU = 3. The reflectance spectrum at t = 0 min corresponds to the dry state. The thickness of the cellulose hydrogel increases with time as water is absorbed. (c) The simulated reflectance spectra of the planar hydrogel MIM etalon for thicknesses from 100 nm to 600 nm. (d-e) SEM images of the cellulose hydrogel film with different ECH:AGU ratios: (d) ECH:AGU = 1 and (e) ECH:AGU = 3. The cellulose hydrogel films were prepared by vacuum freeze-drying. The thicknesses of the dried hydrogel films were 299 ± 24 nm and 170 ± 7 nm respectively. (f) The swelling ratio by weight of the cellulose hydrogel for different ECH/AGU ratios. The ambient temperature was 20 ± 3 °C and the relative humidity was 30 ± 5%.

Because the hydrogel is a porous network, the structure of the network is influenced by the degree of crosslinking. This influences the water absorption properties and therefore the colour changes to the MIM etalon. Figure 4 presents results of experiments on the influence of different chemical crosslinker ratios. The film stacks had thicknesses of 299 ± 24 nm (ECH:AGU = 1) and 170 ± 7 nm (ECH:AGU = 3). The evolution of their optical signatures is shown in Figure 4a and Figure 4b, with SEM images of the dry polymer networks shown in Figure 4d and Figure 4e respectively. It can be seen that, in the first case with ECH:AGU ratio 1, the spectral evolution only involves two orders of resonances, as indicated by the two,

distinct green strokes (Figure 4a), in contrast to the ECH:AGU ratio 3 film, where three orders of resonance in the spectral evolution are evident from the three, distinct, green strokes (Figure 4b). The SEM images show fabric character in both cases. The ECH:AGU ratio 1 sample has a much looser, porous structure. There are obvious pores between the cellulose networks. The networks of the ECH:AGU ratio 3 sample are much denser and more uniform, indicating a better interaction and greater water absorption ability. It has been previously shown ,[43,44] that swelling is a competitive equilibration process, in which the permeation of water into the hydrogel, is balanced by an elastic stretching force, which prevents the deformation of the hydrogel. When these two competing forces are in balance, the swelling stops. It is generally found that a higher chemical crosslinker ratio in the cellulose hydrogel results in a higher swelling ratio.[32,45,46] After leaving the hydrogel in distilled water for one week, we found swelling ratios of 310% and 531% for ECH:AGU ratios of 1 and 3 respectively. Even though the spectral evolution is strongly dependent on the dry thickness and the swelling properties of the hydrogel, it can be located on a general map obtained from simulations (Figure 4c). Here the spectral evolution is shown for MIM film stacks with the hydrogel thickness changing from 100 nm to 600 nm. On the right side, the range of the spectra of Figure 4a and 4b are indicated and the swelling behaviour for the two networks is shown in Figure 4f. Initially, both types of hydrogel exhibit fast water absorption but the rate then plateaus. Faster reflectance changes are also observed in the beginning, followed by a gradual decrease in speed and finally a steady state. For a ECH:AGU = 1 the swelling ratio by weight ($W_{swollen}/W_{dried}$) plateaus at approximately 300% after 20 min, whereas for ratio 3 the swelling ratio plateaus only after 45 min at approximately 510%. This indicates that a denser polymer increases the sensitivity of the optical response. For a long-term stability test we used an etalon containing a hydrogel with ECH:AGU ratio 1 because it has the loosest network. This etalon was characterized after fabrication and then kept in its dried state for 12 months, after which the characterization was repeated (Figure S6). Evidently, the evolution of

the reflection spectra during swelling is largely preserved (Figure 4a), thus showing good stability.

It is important to distinguish the humidity of the hydrogel from the humidity of the environment. To sense relative humidity (Φ) in air, the optical response is governed by the swelling and shrinking of the hydrogel induced by the changing water vapour pressure. We have investigated the shift in optical response versus Φ. The experimental set-up is shown in Figure S7, and the evolution of the reflection spectra for increasing and decreasing values of Φ between 10-90% is shown in Figure S8. Firstly, the position of the interference maximum is red-shifted with increasing Φ indicated by the dashed line (Figure S8a). Subsequently, when the humidity is decreased, a blue-shift is observed (Figure S8b). The shift in maximum position λ_{max} versus Φ is shown in Figure S8c and is comparable to other optical humidity sensors.[47-50] Thus we have demonstrated that an MIM structure offers a scalable and tunable optical humidity sensor. The platform is robust because of both its simple fabrication and its durability. Importantly, chemical modification of the hydrogel offers a pathway to more selective chemical sensing. The only limitation is the rate of molecular transport from the environment into the film but this is not an issue for small MIM structures, for which response times of seconds are easily achieved.

3. Conclusions

We have deposited a double-network cellulose hydrogel between two Au layers, in order to create a flexible MIM etalon. These soft MIM film stacks respond to changes in the refractive index and/or thickness of the hydrogel. As a consequence, distinct structural colour changes can be observed when there are changes in ambient humidity. Analysis of the reflectance spectra revealed continuous and reversible spectral shifts during both swelling and shrinking of the hydrogel. Simulated reflectance spectra support the obtained experimental results and

analysis. The chemical crosslinker ratio has a large influence on the hydration behaviour of the hydrogel with higher chemical crosslinker ratio providing a larger optical response. These bio-hydrogel based MIM film stacks also showed good mechanical stability for up to 12 months. Further functionalisation of these cellulose hydrogels should enable sensors that respond to a variety of external stimuli to be developed.

4. Experimental section

Materials: The cotton linter pulp was supplied by Hubei Chemical Fiber Co. Ltd. (Xiangyang, China). The degree of polymerization (DP) was determined to be 580. Urea, LiOH, and ethyl alcohol of analytical grade were purchased from Ajax Chemicals. Epichlorohydrin (ECH) was purchased from Sigma-Aldrich. Polydimethylsiloxane was purchased from CBC Australia Pty Ltd. All the chemicals were used without further purification.

Fabrication of the planar MIM film stacks : PDMS was used as a substrate. It was prepared by mixing components A and B at a ratio of 10:1 and poured onto a silicon wafer to yield a 2 mm thick film that was cured for 4 h at 75 °C. 100 nm Au was deposited on the PDMS using Electron beam Evaporation (EBE) with an Intlvac Nanochrome II system. The deposition rate was 0.5 Å/s under 9×10^{-6} mbar vacuum. The cellulose hydrogel precursor was prepared by dissolving cotton linter into an aqueous 4.6 wt% LiOH/15 wt% urea solution under continuous stirring (1200 rpm) at −12.5 °C.[39] The concentration of cellulose solution was 3 wt%. The obtained cellulose solution was centrifuged at 7500 rpm for 20 min at 0 °C to remove the impurities from the cotton linter. ECH was injected dropwise by a syringe pump during 2 h into the stirring cellulose solution (1000 rpm at 0°C) until the desired molar ratio of ECH to AGU in the cellulose (i.e., 1, 2, 3) was attained. Air bubbles were then removed by evaporation. The transparent and viscous cellulose solution contained ECH and was used to spin-coat a film onto a 1×1 cm^2 gold-coated PDMS substrate at a spin speed of 8000 rpm for

5 min. This gold/PDMS substrate was preconditioned in an oxygen plasma and cleaned for 90 s. The obtained samples were sealed and maintained at 4 °C for 24 h to allow the hydrogel film to stabilise. After that, the samples were washed with 30 wt% ethanol aqueous solution to remove the urea and LiOH and then left to dry.[12] Finally, a second 30 nm thick Au film was evaporated to complete the assembly of the optical cavity.

Characterization : Bright-field reflection spectroscopy was used to capture the reflection spectra of the planar MIM film stacks, which comprised a Nikon Lv100 Eclipse inverted microscope, equipped with a LU plus ELWD 2 × /0.06 Nikon lens in the reflection configuration. The light source of the microscope was a 100 W quartz halogen lamp. The reflected light was captured by an Acton Micro-Spec 2150i imaging spectrograph fitted with a PIXIS 1024F CCD. A second camera (ThorLabs) was attached to the microscope to capture the bright-field images. An MFP-3D AFM (Asylum Research) Atomic Force Microscope (AFM) was used to measure film thicknesses both in air and in water. Steps in the film were created for this purpose. A SIGMA (Zeiss, Germany) scanning electron microscope (SEM) was used to image the microstructure of the hydrogel films. The swollen hydrogel was freeze-dried and sputter-coated with a thin layer of gold for SEM. The refractive index of the dry cellulose film was obtained from a HORIBA Jobin Yvon UVISEL spectroscopic ellipsometer.

Simulations: The simulations were carried out with the COMSOL Radio Frequency (RF) module. The geometry of the model is shown in Figure S1. The simulation unit cell was 3000 nm in length and 300 nm in width. Periodic boundary conditions were applied to the left and right boundaries. The top boundary of the cell was set to be the input port where the excitation wave was generated with power = 1 W and electric field amplitude = 1 V/m and the bottom boundary of the cell was set to be the port-out for the transmitted wave. The MIM structure was built in the middle of the cell with a 30 nm thick gold slab on the top. The insulator layer had both a varied thickness and refractive index and finally there was a 100

nm gold mirror at the bottom. The refractive index (dielectric permittivity) of gold was adapted from previous reports by Johnson and Christy.[40] The refractive index of the hydrogel was varied as a linear function of its thickness ranging from 1.53 to 1.44 based on the Maxwell-Garnett mixing formula. The wavelength range used was from 500 nm to 900 nm with a 10 nm stepsize and the thickness of the insulator layer ranged from 100 nm to 600 nm, again with a 10 nm stepsize.

Supporting Information

Supporting Information is available from the Wiley Online Library or from the author.

Author Information

Corresponding Authors

*E-mail: mulvaney@unimelb.edu.au. (P. M.), zhoujp325@whu.edu.cn (J. P. Z.)

Notes

The authors declare no competing financial interest.

Author Contribution

Y. D. designed the experiments and experimental devices, built the experiment setup, prepared the hydrogel, analyzed the etalon and co-wrote the manuscript. E. M. A. analyzed the refractive index data, and developed the EMA model and helped write the manuscript. H. Y. Z. carried out the simulations and helped write the manuscript. F. M. carried out nanofabrication of the gold layer by EBE. P.M. and J. P. Z. conceived the research, supervised the research work, and co-wrote the manuscript.

Acknowledgements

This work was financially supported by the ARC through Grant CE170100026 and Chinese Scholarship Council. E.M.A. acknowledges funding by the Alexander von Humboldt Foundation through a Feodor Lynen Research Fellowship. National Natural Science Foundation of China (51473128) has supported the SEM analysis. This work was performed in part at the Melbourne Centre for Nanofabrication (MCN) in the Victorian Node of the Australian National Fabrication Facility (ANFF).

References

[1] A. K. Yetisen, I. Naydenova, F. da Cruz Vasconcellos, J. Blyth, C. R. Lowe, *Chem. Rev.* **2014**, *114*,10654.

[2] M. T. Hill, M. Marell, E. S. Leong, B. Smalbrugge, Y. Zhu, M. Sun, P. J. Van Veldhoven, E. J. Geluk, F. Karouta, Y.-S. Oei, *Optics Express* **2009**, *17*,11107.

[3] J. A. Schuller, E. S. Barnard, W. Cai, Y. C. Jun, J. S. White, M. L. Brongersma, *Nat. Mater.* **2010**, *9*,193.

[4] Y. Nishijima, A. Balcytis, S. Naganuma, G. Seniutinas, S. Juodkazis, *ACS Appl. Nano Mater.* **2018**, *1*,3557.

[5] Z. Liu, G. Liu, X. Liu, Y. Wang, G. Fu, *Opt. Mater.* **2018**, *83*,118.

[6] K. Aydin, V. E. Ferry, R. M. Briggs, H. A. Atwater, *Nat. Commun.* 2011, 2,517.

[7] E.-S. Yu, S.-H. Lee, Y.-G. Bae, J. Choi, D. Lee, C. Kim, T. Lee, S.-Y. Lee, S.-D. Lee, Y.-S. Ryu, *ACS Appl. Mater. Inter.* **2018**, *10*, 38581.

[8] C. D. Sorrell, M. J. Serpe, *Adv. Mater.* **2011**, *23*, 4088.

[9] R. J. Walters, R. V. van Loon, I. Brunets, J. Schmitz, A. Polman, *Nat. Mater.* **2010**, *9*,21.

[10] A. H. Alshehri, K. Mistry, V. H. Nguyen, K. H. Ibrahim, D. Muñoz-Rojas, M. Yavuz, K. P. Musselman, *Adv. Funct. Mater.* **2019**, *29*, 1805533.

[11] E. W. Cowell, N. Alimardani, C. C. Knutson, Jr J. F. Conley, D. A. Keszler, B. J. Gibbons, J. F. Wager, *Adv. Mater.* **2011**, *23*, 74.

[12] K.-E. You, N. Uddin, T. H. Kim, Q.-H. Fan, H. J. Yoon, *Sensor Actuat. B-Chem.* **2018**, *277*, 62.

[13] H. Moon, H. Seong, W. C. Shin, W. T. Park, M. Kim, S. Lee, J.-H. Bong, Y. Y. Noh, B. J. Cho, S. Yoo, S. G. Im, Nat. Mater. **2015**, *14*, 628.

[14] H. Fudouzi, T. Sawada, *Langmuir* **2006**, *22*, 1365.

[15] H. Kwon, S. Kim, *ACS Photonics* **2015**, *2*, 1675.

[16] C. Ma, W. Lu, X. Yang, J. He, X. Le, L. Wang, J. Zhang, M. J. Serpe, Y. Huang, T. Chen, *Adv. Funct. Mater.* **2018**, *28*, 1704568.

[17] Q. Wang, J. Guo, Z. Ding, D. Qi, J. Jiang, Z. Wang, W. Chen, Y. Xiang, W. Zhang, A. T. Wee, *Nano lett.* **2017**, *17*, 7593.

[18] O. B. Ayyub, P. Kofinas, *ACS nano* **2015**, *9*, 8004.

[19] R. Takahashi, T. L. Sun, Y. Saruwatari, T. Kurokawa, D. R. King, J. P. Gong, *Adv. Mater.* **2018**, *30*, e1706885.

[20] T. Nezakati, A. Seifalian, A. Tan, A. M. Seifalian, *Chem. Rev.* **2018**, *118*, 6766.

[21] A. S. Carlini, L. Adamiak, N. C. Gianneschi, *Macromolecules* **2016**, *49*, 4379.

[22] Y. Liu, Y. Sui, C. Liu, C. Liu, M. Wu, B. Li, Y. Li, *Carbohyd. Polym.* **2018**, *188*, 27.

[23] B. Mandal, A. P. Rameshbabu, S. R. Soni, A. Ghosh, S. Dhara, S. Pal, *ACS Appl. Mater. Inter.* **2017**, *9*, 36583.

[24] R. E. Abouzeid, R. Khiari, D. Beneventi, A. Dufresne, *Biomacromolecules* **2018**, *19*, 4442.

[25] S. Sultan, A. P. Mathew, *Nanoscale* **2018**, *10*, 4421.

[26] K. Bethke, S. Palantöken, V. Andrei, M. Roß, V. S. Raghuwanshi, F. Kettemann, K. Greis, T. T. K. Ingber, J. B. Stückrath, S. Valiyaveettil, K. Rademann, *Adv. Funct. Mater.* **2018**, *28*, 1800409.

[27] H. Sai, R. Fu, L. Xing, J. Xiang, Z. Li, F. Li, T. Zhang, *ACS Appl. Mater. Inter.* **2015**, *7*, 7373.

[28] N. Zhao, F. Wu, Y. Xing, W. Qu, N. Chen, Y. Shang, M. Yan, Y. Li, L. Li; R. Chen, *ACS Appl. Mater. Inter.* **2019**, *11*, 15537.

[29] H. Cheng, Y. Du, B. Wang, Z. Mao, H. Xu, L. Zhang, Y. Zhong, W. Jiang, L. Wang, X. Sui, *Chem. Eng. J.* **2018**, *338*, 1.

[30] W. Song, J. K. Lee, M. S. Gong, K. Heo, W. J. Chung, B. Y. Lee, *ACS Appl. Mater. Inter.* **2018**, *10*, 10353.

[31] Y. Shang, Z. Chen, F. Fu, L. Sun, C. Shao, W. Jin, H. Liu, Y. Zhao, *ACS Nano* **2019**, *13*, 796.

[32] D. Zhao, J. Huang, Y. Zhong, K. Li, L. Zhang, J. Cai, *Adv. Funct. Mater.* **2016**, *26*, 6279.

[33] L. S. Sobhanadhas, L. Kesavan, P. Fardim, *Langmuir* **2018**, *34*, 9857.

[34] C. Chang, L. Zhang, J. Zhou, L. Zhang, J. F. Kennedy, *Carbohyd. Polym.* **2010**, *82*, 122.

[35] H. Zheng, W. Li, W. Li, X. Wang, Z. Tang, S. X. Zhang, Y. Xu, *Adv. Mater.* **2018**, *30*, e1705948.

[36] A. P. C. Almeida, J. P. Canejo, S. N. Fernandes, C. Echeverria, P. L. Almeida, M. H. Godinho, *Adv. Mater.* **2018**, *30*, e1703655.

[37] C. Fabry, A. Pérot, *Ann. Chim. Ser.* **1899**, *16*, 115.

[38] Z. Wang, X. Liu, Y. Wu, B. Liu, Z. Wang, J. Zhang, K. Liu, B. Yang, *J. Mater. Chem. C* **2018**, *6*, 10861.

[39] J. Cai, L. Zhang, *Macromol. Biosci.* **2005**, *5*, 539.

[40] P. B. Johnson, R. W. Christy, *Phys. Rev. B* **1972**, *6*, 4370.

[41] K. Kurokawa, *IEEE Trans. Microw. Theory Tech.* **1965**,13, 194.

[42] J. P. Gong, Y. Katsuyama, T. Kurokawa, Y. Osada, *Adv. Mater.* **2003**,*15*, 1155.

[43] F. Ganji, S. Vasheghani-Farahani, E. Vasheghani-Farahani, *Iran. Polym. J.* **2010**, *19*, 375.

[44] E. C. Achilleos, R. K. Prud'homme, K. N. Christodoulou, K. R. Gee, I. G. Kevrekidis, *Chem. Eng. Sci.* **2000**, *55*, 3335.

[45] J. P. Gong, *Soft Matter*, **2010**, *6*, 2583.

[46] D. Xu, J. Huang, D. Zhao, B. Ding, L. Zhang, J. Cai, *Adv. Mater.* **2016**, *28*, 5844.

[47] F. J. Arregui, Y. Liu, I. R. Matias, R. O. Claus, *Sensor Actuat. B* **1999**,*59*, 54.

[48] L. H. Chen, T. Li, C. C. Chan, R. Menon, P. Balamurali, M. Shaillender, B. Neu, X. M. Ang, P. Zu, W. C. Wong, K. C. Leong, *Sensor Actuat. B-Chem.* **2012**, *169*, 167.

[49] J. S. Santos, I. M. Raimundo Jr., C. M. B. Cordeiro, C. R. Biazoli, C. A. J. Gouveia, P. A. S. Jorge, *Sensor Actuat. B-Chem.* **2014**, *196*, 99.

[50] D. Su, X. Qiao, Q. Rong, H. Sun, J. Zhang, Z. Bai, Y. Du, D. Feng, Y. Wang, M. Hu, Z. Feng, *Opt. Commun.* **2013**, *311*, 107.

Table of Contents: A Fabry-Pérot type soft optical etalon was made by introducing cellulose hydrogel as the insulating layer. The etalon changes colour in response to changes in the hydrogel thickness or refractive index. This forms the basis for a robust, optically based, portable, humidity and chemical sensor.

Keywords: MIM devices, soft etalon, cellulose, hydrogels

Yue Dong, Eser Metin Akinoglu, Heyou Zhang, Fatemeh Maasoumi, Jinping Zhou and Paul Mulvaney**

An Optically Responsive Soft Etalon Based on Ultrathin Cellulose Hydrogels